29th AIAA Applied Aerodynamics Conference
27 - 30 June 2011, Honolulu, Hawaii

AIAA 2011-3521

High-Fidelity Optimization of Flapping Airfoils and Wings

Matthew Culbreth,* Yves Allaneau* and Antony Jameson†
Stanford University, Stanford, CA 94305, USA

We present the results of several optimizations for 2D airfoils and 3D wings undergoing periodic, flapping-type motions. Optimizations are achieved by coupling high-fidelity 2D and 3D Navier-Stokes solvers with a gradient-based optimization algorithm. In 2D we consider a pitching and plunging NACA0012 airfoil and investigate the maximization of the propulsive efficiency. In 3D we consider a rectangular wing that is hinged at the root. The motion of the 3D wing is parameterized by spline control points that allow span-wise variation of both the dihedral angle and twist angle, allowing complex wing motions and deformations with relatively few parameters. Propulsive efficiency is maximized for the 3D wing in an non-twisting case as well as using one, two and four of these span-wise twist control points. The results of the optimizations lead to several conclusions, including that pitching and twisting can significantly improve the attainable propulsive efficiency, can delay the onset of leading edge separation, and that solutions that maximize propulsive efficiency appear to operate at the limit of leading edge separation.

Nomenclature

f	Frequency of oscillation
α	Pitch Angle (2D) and twist angle (3D)
θ	Dihedral Angle (3D)
h	Plunging amplitude (2D)
ϕ	Phase offset corresponding to α
ψ	Phase offset corresponding to θ
η_m	Modified propulsive efficiency
P	Aerodynamic power
C_L	Lift coefficient
C_D	Drag coefficient
$\mathbf{x}$	Vector of optimization parameters
$f(\mathbf{x})$	Optimization objective function
$\mathbf{g}(\mathbf{x})$	Non-linear constrain functions
$\mathbf{Ax}$	Linear optimization constraints
$\mathbf{l}$	Lower optimization constrain bound
$\mathbf{u}$	Upper optimization constrain bound

Subscript

x, y, z	Coordinate directions
k, l	Value at k^{th} or l_{th} control points for the dihedral or twist angle, respectively

*Doctoral Candidate, Department of Aeronautics & Astronautics, Stanford University, AIAA Member
†Professor, Department of Aeronautics & Astronautics, Stanford University, AIAA Fellow

I. Introduction

There has been a significant increase in research interest in the aerodynamics of flapping wings within the last decade. Flapping wing flight has become a significant engineering research direction, with the miniaturization of electronic components and increases in battery energy density allowing for the creation of a class of small-scale unmanned flying vehicles generally referred to as micro air vehicles (MAVs). Flapping wings are of particular interest for this application both because of the numerous, highly-successful examples of flapping wing flight found in nature and because flapping wings provide an attractive flight system that provides lifting, thrust and control in a single package. Investigation of flapping wing flight is also of significant importance to the fundamental science of aerodynamics. The development of aircraft over the last century has provided a significant and mature body of understanding of the physics of steady-state fluid dynamics across a wide range of flight speeds. This work generally has little application, however, to the complex and unsteady flapping wing flight regime. Fortunately, high-fidelity computational tools and associated powerful computational hardware now allow for accurate simulation of flapping wings, making it possible to begin to understand the physics of this type of flight. These high-fidelity simulation tools have also opened new possibilities for research into the fluid dynamics of bird and insect flight within the biology community. These tools now allow detailed examination in areas such as the relationship between the kinematics and the resulting forces such as lift and thrust and the flow physics associated with the numerous examples of animal flight mechanisms.

Flapping wing flight is complex and difficult from a research and design stand-point. As previously mentioned, very few of the efficient computational design tools used for large aircraft design can be used in the unsteady, low Reynolds number regime. Accurate simulation of flapping wings requiring costly unsteady numerical flow simulations that can accommodate large mesh motions and deformations and feature low numerical dissipation to accurately capture the complex, vortex dominated flow physics. A second difficulty is that there are many degrees of freedom in the parameterization of flapping wing motions when considering a flexible wing in a generalized periodic flapping motion. While much has been learned from observing the flight of birds and insects, it is still far from clear how to couple wing flexibility and flapping motion in an efficient or optimal way for a given flight performance metric. Additionally, it is not clear how to compactly parameterize flapping wing motion while still retaining the appropriate level of complexity of motion required for efficient flight.

We propose to address the issues associated with selecting an appropriate parameterization and then identifying the parameter values that yield efficient performance by using a numerical optimization process. We have developed 2D and 3D viscous flow solvers that are specifically tailored to simulating a flapping wing. These codes are coupled to a gradient-based numerical optimization algorithm. The optimization process is then used in conjunction with parameterizations of varying complexity to both identify optimal flapping motions and also investigate the trade-off between the complexity of the motion and the attainable performance. In this paper we specifically address the optimization of propulsive efficiency in the 2D and 3D case. In 2D we investigate the pitching and plunging airfoil case. In 3D we investigate a flapping and twisting wing that is hinged at the wing root and has varying degrees of complexity of span-wise twist. We compare the results of these optimizations both to understand the attainable limits of propulsive efficiency and the cost versus benefit of adding additional degrees of freedom to the wing motion.

Background

The study of flapping wings dates back to the beginnings of the study of aerodynamics itself , with attempts at constructing flapping wing vehicles that predate the first powered aircraft. The development of the theory of flapping wings through the twentieth century was somewhat of a footnote in the evolution of aerodynamic theory, which was largely driven by understanding transonic and supersonic fixed-wing flight. Early examples of flapping wing theory come from the work of Theodorsen[1] and Garrick,[2] who developed analytic models for airfoils undergoing small-amplitude oscillations in 2D potential flow, work that was largely motivated by attempts to understand aeroelastic flutter. Lighthill[3] and Weis-Fogh,[4] among others, performed pioneering research on the aerodynamics of biological fliers including the elucidation of some of the complex aerodynamic mechanisms used by these creatures. Interest in flapping flight increased significantly towards the end of the twentieth century as steady aerodynamic theory reached maturity and improvements in algorithms for computational fluid dynamics (CFD) and increasing computing power made higher-fidelity simulations of flapping wings possible. Early numerical simulations of flapping wings were carried out using

unsteady vortex-lattice and panel methods.[5,6] Current computational capabilities allow for high-fidelity, 3D, unsteady Navier-Stokes simulations of flapping wings. A number of detailed CFD studies have been completed, including work by Jones, *et. al.*,[7,8] Shyy *et. al.*,[11] Persson *et. al.*,[9] and Ou *et. al.*[10]

There has also been long-standing research interest in optimization of flapping flight, based partially on the assumption that natural fliers operate in a manner that is optimal in some sense. R.T. Jones[12] developed an expression for the optimal lift distribution along the wing during flapping motion by minimizing induced drag for a given wing bending moment in potential flow. Hall and Hall[13] compute the optimal span-wise circulation distribution on a thrusting and lifting wing using a 1D integral solution in the small amplitude case and a vortex-lattice code in the large amplitude case. Hamdaoui *et. al*[14] use a multi-objective evolutionary algorithm coupled with analytic flapping wing models to optimize various flight metrics. Ito[15] couples a vortex-lattice model with a hybrid optimization method that combines a genetic algorithm with a sequential quadratic programming algorithm. Strang[16] utilizes a vortex-lattice code in conjunction with the gradient-based optimization to investigate the optimal flapping gait of a Pterosaur wing. Milano and Gharib[17] couple a genetic algorithm to an experimental apparatus with a two degree of freedom flapping rectangular plate to maximize average lift force. Tuncer and Kaya[18] use gradient-based optimization coupled with a 2D overset-grid Navier-Stokes solver to maximize thrust and propulsive efficiency of a pitching and plunging airfoil. Willis *et. al.*[19] uses a multi-fidelity approach to optimize flapping wing performance metrics. In their work, flapping motions are generated using optimal wake vorticity distributions generated by a wake only method, which are then further refined using a panel method and finally verified using a Discontinuous Galerkin-based 3D Navier-Stokes solver.

In this work we propose to couple a 3D Navier-Stokes solver with a gradient-based optimization in order create a framework for investigating various combinations of flapping motions and optimization objectives. The details of this framework and several optimization results are presented in the remained of this document.

II. Optimization Framework

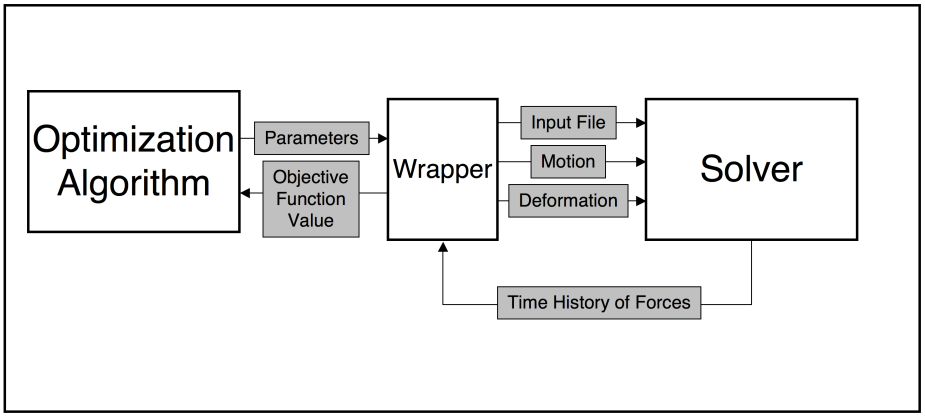

Figure 1. Software block diagram

A block diagram of the software framework for solving flapping-wing optimization problems is shown in figure 1. The two major components are the optimization algorithm and the flow solver, with a "wrapper" that mainly serves as a light-weight interface between these two larger pieces of software. Details of the flow

solver and optimization algorithm, as well as the formulation of the optimization problems are discussed in the remainder of this section.

2D and 3D Navier-Stokes Solvers

The 2D and 3D flow solvers are based on the low-dissipation kinetic energy preserving (KEP) finite volume scheme developed by Jameson[20,21] and extended by Allaneau and Jameson.[22] The kinetic energy preserving property of this scheme allows stability to be maintained with little or no artificial dissipation. This property is especially desirable for vortex dominated flows such as flapping flight since artificial dissipation tends to quickly and unnaturally dampen complex flow features. These codes have been specifically developed to simulate oscillating airfoils and flapping wings and to be integrated into an optimization framework. The full details of this code can be found in the work of Allaneau *et. al.*[23]

A TVD Runge-Kutta second-order multistage time stepping scheme[24] is used for time integration. Structured grids are used throughout, with 2D cases using a C-mesh and 3D cases using a C-H mesh. Both the 2D and 3D solvers allow for mesh motion, with the 2D solver allowing rigid-body transformations of the mesh (enabling pitching and plunging motions), and the 3D solver allowing both rigid transformation and complex deformations of the mesh. The mesh deformations in 3D allow for a wide range of parameterized shape changes, such as wing bending and twisting as well as planform variations, among many other possibilities. Deformations in 3D are accomplished in a computationally inexpensive manner using analytic transformations to a base, undeformed mesh via shearing, stretching and twisting operations. Examples of bending and twisting mesh deformations are shown in figure 2.

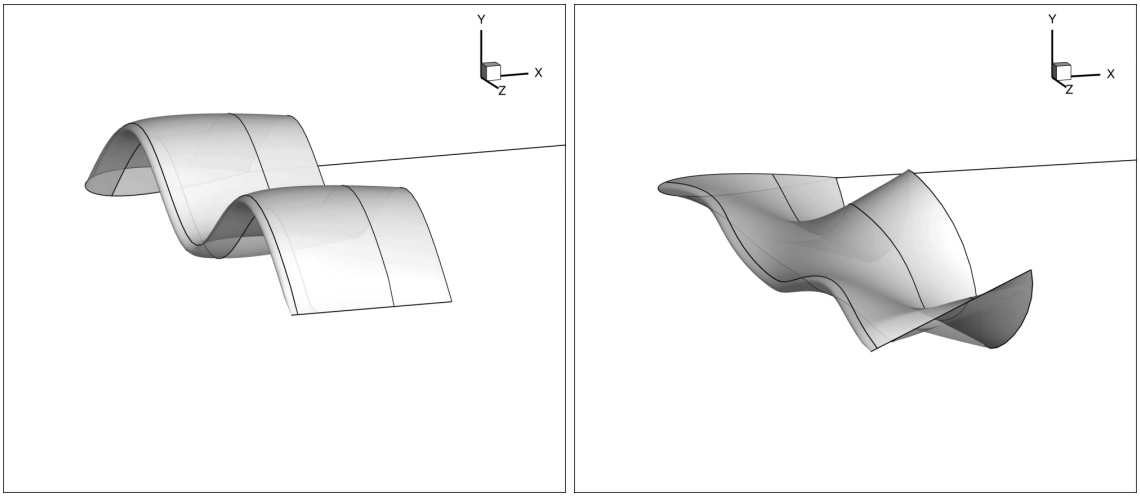

Figure 2. Examples of 3D mesh deformation capabilities in the Navier-Stokes solver

Optimization Problem

We consider a constrained, non-linear optimization problem of the form

$$\begin{aligned} &\text{minimize} && f(\mathbf{x}) \\ &\text{subject to} && \mathbf{l} \leq \begin{pmatrix} \mathbf{x} \\ \mathbf{g}(\mathbf{x}) \\ \mathbf{A}\mathbf{x} \end{pmatrix} \leq \mathbf{u} \end{aligned} \tag{1}$$

where f is the optimization objective function, $\mathbf{x}$ are the optimization parameters, $\mathbf{g}(\mathbf{x})$ are non-linear constraint functions, $\mathbf{A}$ is a matrix of linear constraints on $\mathbf{x}$, and $\mathbf{l}$ and $\mathbf{u}$ are the lower and upper constraint bounds. The optimization variables $\mathbf{x}$ parameterizes the motion and geometry of the flapping wing and $f(\mathbf{x})$ and $\mathbf{g}(\mathbf{x})$ are functions of the time-averages of the force and power coefficients calculated by the flow solver. Details of the parameterization, the objective functions and the optimization algorithm for the 2D and 3D optimizations are given in the remainder of this section.

Parameterizations

In the 2D case we consider single-mode sinusoidal pitching and plunging motions. In the general case these motions take the form

$$\alpha(t) = \alpha_0 + \alpha \cos(2\pi f t + \phi) \tag{2}$$

$$h(t) = h \cos(2\pi f t) \tag{3}$$

The parameterization used in all cases considered herein consists of four optimization variables: the frequency f, the pitch and plunge amplitudes α and h and the phase difference between pitch and plunge ϕ. The base angle of attack α_0 is set to zero in all cases, yielding motions that are symmetric about the axis of free-stream flow.

The 3D motion parameterization is intended to mimic typical flapping motions with combinations of varying dihedral angle at the wing root and twisting along the span. Smooth variation of the dihedral angle $\theta(s)$ and the twist angle $\alpha(s)$ (where s is the span-wise arc-length parameter) are generated by fitting piece-wise cubic splines through one or more control points along the span. Illustrations of the spline control points for dihedral angle and twist are show in figure 3. For the resulting surface deformation refer again to figure 2.

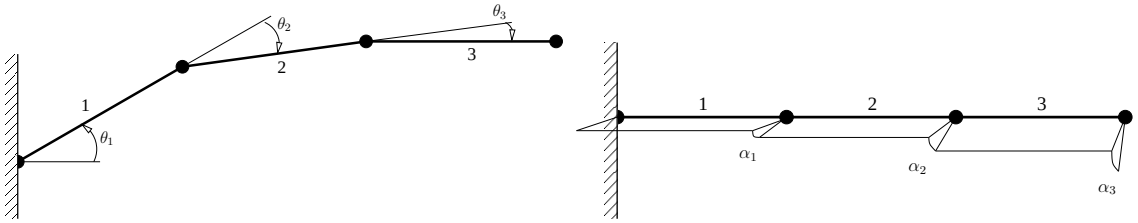

Figure 3. Illustration of the 3D flapping parameterizations showing the dihedral angle (left) and the twist angle (right)

The time-dependent flapping motion is parameterized by prescribing sinusoidal variation to a set of k dihedral control points and l twist control points spaced evenly along the span. Each control point maintains a parameter for the incremental dihedral angle θ_k and the incremental twist α_l along with associated phase angles ϕ_k for the flap angle and ψ_l for the twist angle. The equations of motion are of the form

$$\theta_k(t) = \theta_k \cos(2\pi f t + \phi_k) \tag{4}$$

$$\alpha_l(t) = \alpha_l \cos(2\pi f t + \psi_l) \tag{5}$$

The complete motion of the wing is parameterized by the frequency f, the dihedral and twist angles θ_k and α_l, and the dihedral and twist phase angles ϕ_k and ψ_l for $k = 1 \ldots m$ and $l = 1 \ldots n$ control points and resulting in $2m + 2n + 1$ total optimization parameters.

Components of the Objective Functions and Constraints

Objective functions are based on time-averages of various integrated force and power coefficients calculated by the flow solver. These include the average lift $\overline{C_L}$, average thrust $\overline{C_T} = -\overline{C_D}$ and the aerodynamic power averages $\overline{P_x}$, $\overline{P_y}$ and $\overline{P_z}$. We also differentiate between the thrust-producing power $\overline{P_x} = U_\infty \overline{C_T}$ and the non-thrust-producing powers $\overline{P_y}$ and $\overline{P_z}$. In all cases these averages are computed by integrating over a single flapping cycle after a suitable number of periods have elapsed to allow the flow to reach a quasi- periodic state.

Propulsive efficiency is a commonly used performance metric in propellers and flapping wing systems and the maximization of propulsive efficiency is an attractive objective function for the optimization of these systems. The propulsive efficiency is the ratio of thrust-producing power to the mechanical power required to flap the wing or to pitch and plunge the airfoil. However, as first observed by Jones and Platzer,[6] the propulsive efficiency is a discontinuous function. Furthermore, the discontinuity occurs in the vicinity of the maximum propulsive efficiency, making it a very difficult problem for many optimization algorithms. For this reason we use a "modified propulsive efficiency" η_m given by

$$\eta_m = \frac{P_x}{\sqrt{P_x^2 + P_y^2 + P_z^2}} \tag{6}$$

This formulation removes the problem of a discontinuous objective function since, for all practical cases, $\sqrt{P_x^2 + P_y^2 + P_z^2} > 0$.

Optimization Algorithm

A single objective function evaluation requires a time-accurate solution from the 2D or 3D flow solver. These solutions are computed on large clusters and typically use between 64 and 512 compute cores. However, even with these significant compute resources flow solutions take on the order of several hours. The significant computational cost of objective function evaluations motivates the use of a gradient-based optimization algorithm since these methods tend to require far fewer evaluations of the objective functions than gradient-free methods such as genetic algorithms so long as the objective function is locally smooth near the optimum. We have chosen to use the SNOPT package[25] for all of the optimizations presented here. SNOPT is a widely used software library based on the sequential quadratic programming (SQP) method and is designed for use on constrained, non-linear optimization problems. Gradients are computed within SNOPT via finite-differences, which require on the order of n function evaluations per gradient calculation. The calculation of the gradients dominates the computational cost for all but the smallest problems, however since the function evaluations within each gradient calculations are independent the process can be parallelized.

III. 2D Optimizations

For the 2D pitching and plunging airfoil case we consider the maximization of the modified propulsive efficiency using a NACA0012 airfoil at a Reynolds number of 1850 based on the chord and a mach number of 0.2. The numerical solutions for all 2D cases use a 1024×128 C-mesh and are integrated over five periods to ensure that the force and power reach a periodic state. The force and power coefficients are integrated over the final oscillation cycle to obtain the averaged quantities for the objective function. The solver is run in parallel on a large cluster, typically using 64 compute cores per flow solution. Compute times are on the order of 2 hours per flow solution. Optimal solutions are validated using a 4096×512 mesh that is effectively DNS resolution for the given Reynolds number.

The parameter values for the optimal cases are given in table 1. Figure 5 show the contours of vorticity magnitude at four points in the flapping cycle. Figure 4 contains the lift versus drag coefficient polars over one flapping cycle.

Table 1. Optimal parameters for 2D maximization of modified propulsive efficiency

Case	Frequency	α	h	ϕ	η_m
Plunging	2.63 Hz	-	0.252	-	**12.1**%
Pitching/Plunging	4.61 Hz	19.78°	0.212	67.03°	**31.4**%

The results from the optimizations show that an increase in modified propulsive efficiency from 12.1% to a maximum of $\eta_m = 31.4\%$ is achieved by adding the pitching degree of freedom, and it is also interesting to note that the frequency nearly doubles for the pitching and plunging case. The lift versus drag polars in figure 4 give insight into the differences between these two cases. Non-lifting cases with $\eta_m = 100\%$ must all lie along the line $C_L = 0$ since P_y and P_z must be everywhere zero. The efficiency of a given flapping cycle can then generally be inferred by observing the aspect ratio of the polar. The wider and the polar along C_D and the narrower along C_L, the greater the magnitude of η_m, and additionally, for η_m to be positive the polar must show a net thrust. This is seen in figure 4 where the pitching and plunging case shows a significant increase in thrust production compared with the plunging case with only a relatively small increase in lift through the cycle.

The vorticity contours in figure 5 show the formation of significant leading-edge vortices on the up and down stroke in the plunging case. The pitching and plunging case, however, shows an absence of leading edge vortex formation. Close examination of the pitching and plunging case shows the formation of a small separation bubble that appears near the leading edge of the airfoil at the beginning of the up and down strokes and moves aft as the stroke progresses, but does not develop into a vortex. The formation of this separation bubble indicates that the flow is likely on the verge of stalling, which would lead to the formation of a full leading-edge vortex. This indicates that a characteristic of maximum propulsive efficiency in the 2D

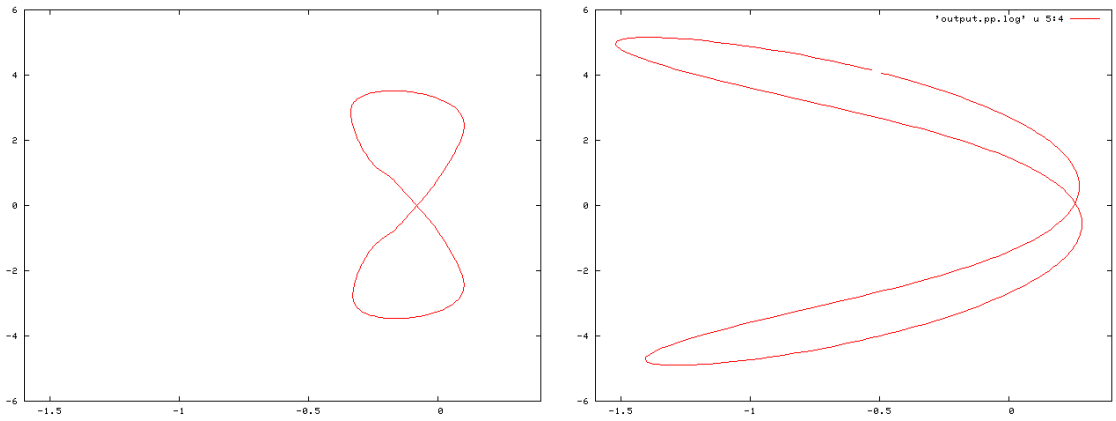

Figure 4. C_L versus C_D polars for optimal 2D cases. The vertical axis represent lift and the horizontal axis represents drag. The left plot shows the polar for the plunging case and the right plot shows the polar for the pitching and plunging case.

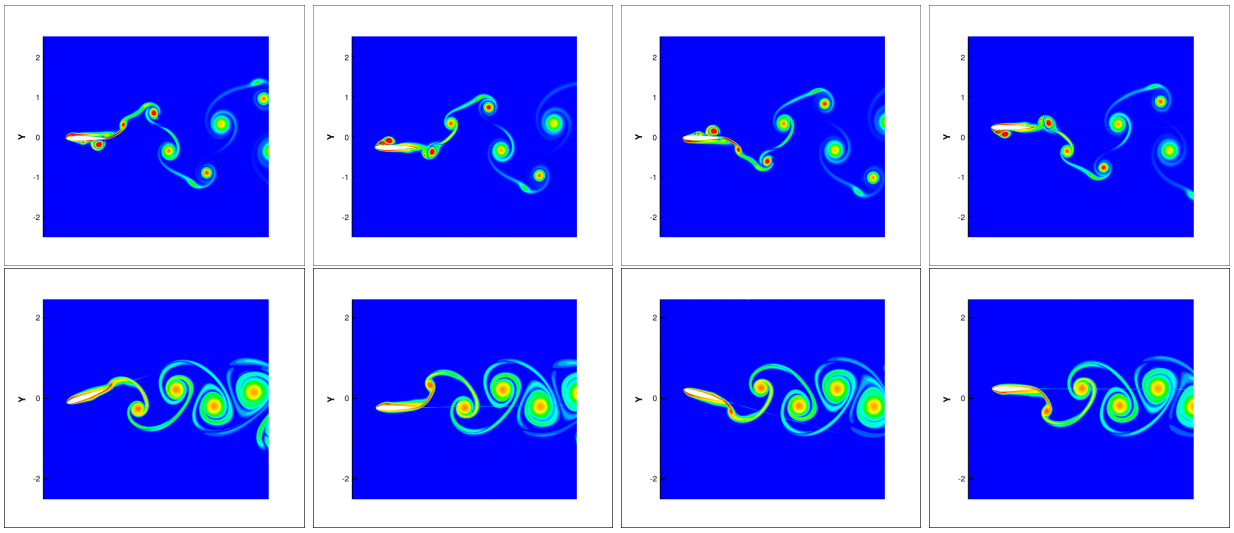

Figure 5. Vorticity visualization of the flapping cycle for maximum propulsive efficiency. The top row depicts the plunging case and the bottom row depicts the pitching and plunging case. Note that the vorticity contour colormaps values are not quite the same between the top and bottom rows.

case is that the motion drives the flow to the limit of separation without exceeding it, which would cause a drop in suction and dissipate of excessive energy into the flow by forming a vortex.

IV. 3D Optimizations

For the 3D flapping wing case we consider the maximization of propulsive efficiency with increasing numbers of span-wise control points. The wing configuration in all cases has a rectangular planform with an aspect ratio of 8 and a NACA0012 airfoil section. The domain is discretized using an H-C mesh with $256 \times 64 \times 64$ cells and employs a symmetry plane. A mach number of 0.2 and a Reynolds number of 2000 based on the chord length are used throughout and flow solutions are integrated over five flapping cycles, with the averaged force and power coefficients being integrated over the final flapping cycle. Flow solutions are run in parallel, typically using 256 cores, requiring approximately 3-4 hours of wall-time per simulation.

We present results for four cases with a single dihedral control point ($k = 1$) and zero, one, two and four evenly spaced twist control points along the span ($l = 0, 1, 2, 4$). The $l = 0$ case yields purely dihedral oscillation and is akin to the plunging airfoil case in 2D. The $l = 1, 2\&4$ are akin to the pitching and plunging case in 2D with increasing complexity of spanwise twist distribution. In the $l = 4$ case the optimization

algorithm failed to improve on the results from the $l = 2$ case, and so further results from this case are not included. Table 2 contains a summary of the 3D optimizations. Figure 6 shows the wing geometry for each case with surface pressure contours at four points over one flapping cycle. Figure 7 shows the same plots with vorticity isosurfaces overlaid. Figure 8 shows the lift versus drag coefficient polars over one flapping cycle.

Table 2. Summary of 3D maximization of propulsive efficiency for varying numbers of span-wise control points

Control Points	Frequency	θ	Cumulative Twist	η_m
0	3.626 Hz	6.53°	–	**9.60**%
1	0.641 Hz	46.9°	62.5°	**46.7**%
2	0.755 Hz	47.1°	58.4°	**49.5**%
4	–	–	–	No Improvement

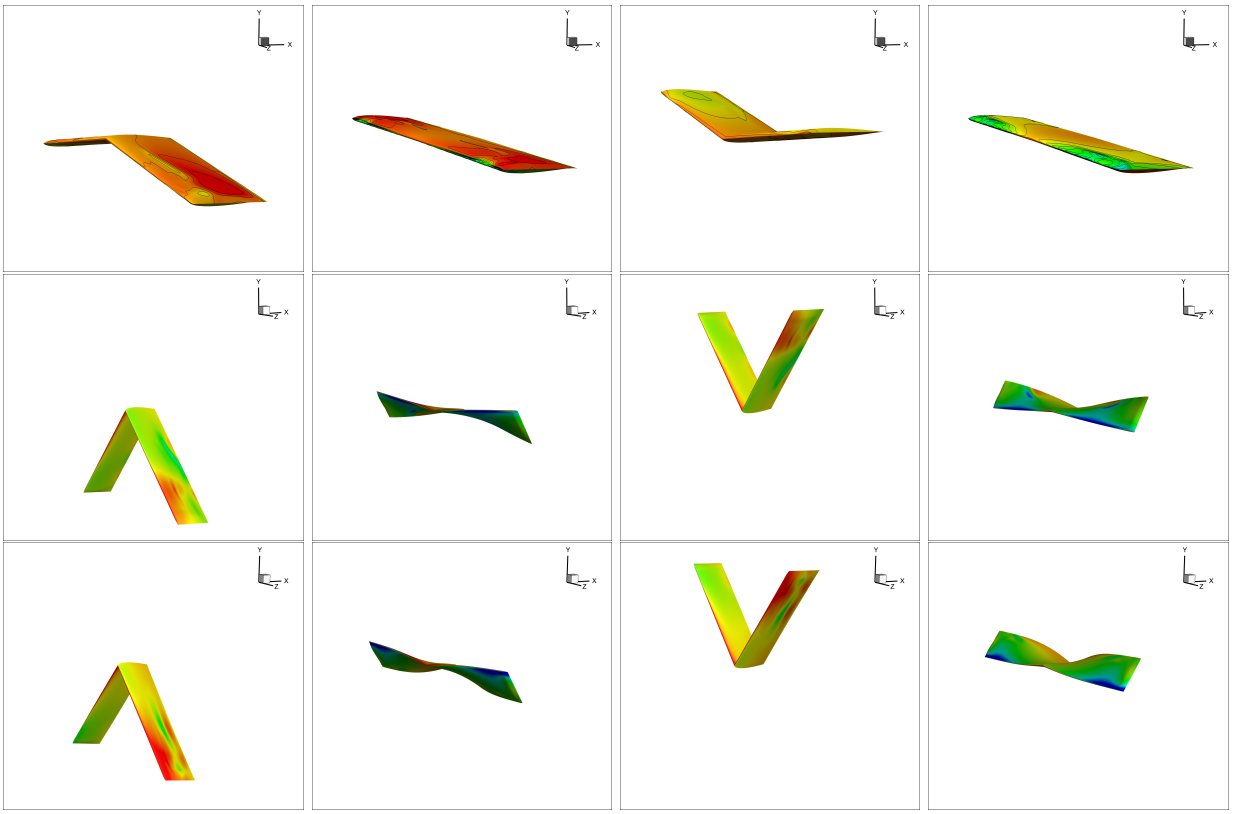

Figure 6. Vorticity isosurface visualization of the flapping cycle for maximum propulsive efficiency. Color values are based on pressure. The top row depicts the case without twisting motion, the middle row depicts the case with one twist control point, and the bottom row depicts the case with two twist control points.

The 3D results show that the addition of wing twist produces a significant improvement in the modified propulsive efficiency, increasing the propulsive efficiency from around 10% to almost 47% by allowing linear twist. The efficiency is further improved to nearly 50% by allowing for a more complex and non-linear twist distribution. There is also a significant decrease in frequency and increase in dihedral amplitude between the $l = 0$ and $l = 1$ cases, while there is a relatively minor change in the motion between the $l = 1$ and $l = 2$ cases. All phase angles, which have been omitted for brevity, are within the range $90° \pm 10°$.

Figure 6 further illustrates the significant difference in the dihedral amplitude between the twist-free case and the twisting cases, while there is little discernible difference in the twist distribution with one versus two twist control points. Further analysis of the $l = 2$ case indicates that the twist angle reaches approximately 78% of the final tip twist angle of 58.4° between the wing root and the mid-span control point, with relatively little additional twist occurring between mid-span and the wing tip.

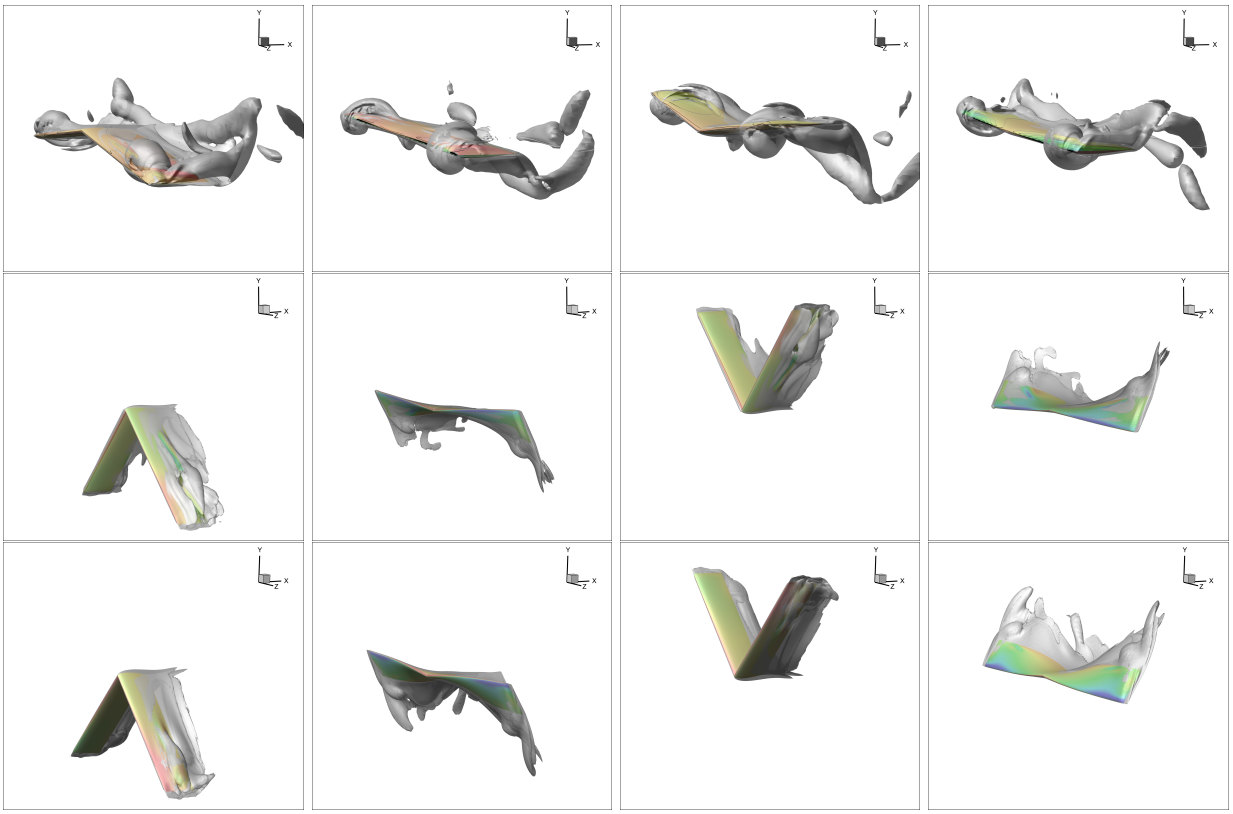

Figure 7. Vorticity isosurface visualization of the flapping cycle for maximum propulsive efficiency. Color values are based on pressure. The top row depicts the case without twisting motion, the middle row depicts the case with one twist control point, and the bottom row depicts the case with two twist control points.

The vorticity isosurface plots in figure 7 provide some insight into the flow physics of the different cases. The twist-free case shows evidence of significant leading edge separation during the up and down strokes towards the wing tips, while the plots for the twisting cases indicate much less leading edge separation. The twisting cases appear demonstrate some instability or separation bubble formation, with the $l = 2$ case appearing to reduce the severity of the instability over the $l = 1$ case. These findings are similar to the findings in the 2D cases in that the addition of pitching/twisting improves efficiency by apparently reducing or eliminating leading edge separation, and that high propulsive efficiencies are achieved by motions that are at the limit of leading edge separation.

The polar plot in figure 8 also show trends that are similar to the 2D case. The polar for the twist-free case has a large C_L range and a low-magnitude but largely negative (thrust producing) C_D range resulting in low efficiency. The twisting cases show a reduced C_L and increased thrust, both contributing to the increase in efficiency. Between the $l = 1$ and $l = 2$ cases the maximum thrust coefficient increases from approximately 0.8 to 1.2 without a significant change in the C_L range. A noted difference between the 2D and 3D cases is that, while in the 2D case the C_L range increases for the pitching and plunging case, in 3D the C_L range decreases for the twisting cases. It is not clear if this is a result of the fundamental difference between 2D and 3D flows, or if it an indication of potential room for further optimization of the 2D results.

V. Conclusion

Our results show that significant improvements are made to propulsive efficiency of by introducing pitching motion in 2D and twisting motion in 3D. The physical mechanism for this improvement in both cases appears to be the elimination of the inefficient leading edge vortex by providing instantaneous angle of attack relief with respect to the motion of the wing or airfoil. The airfoil and wing both appear to be on the verge of forming leading edge vortices as evidenced by the appearance of separation bubbles and instabilities in plots of vorticity. Overall, results show that pitching/twisting are important mechanisms for producing efficient

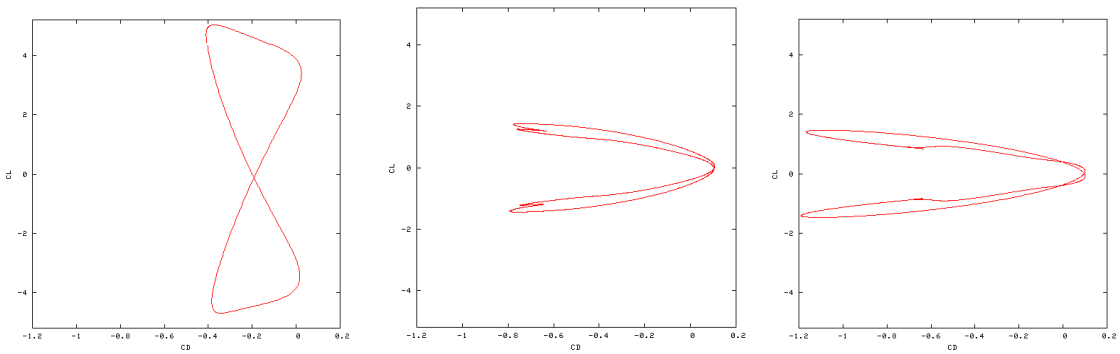

Figure 8. C_L **versus** C_D **polars for optimal 3D cases. The vertical axis represent lift and the horizontal axis represents drag. The left plot shows the polar for the non-twisting case, the center plot shows the polar for the single control point case and the right plot shows the polar for the 2 control point case.**

thrust in flapping flight. In the 2D parameterizations the addition of two parameters to represent the amplitude and phase of a simple sinusoidal pitching or linear twisting motion provides significant improvements in the maximum attainable propulsive efficiency over the cases without these motions. The 3D results show that further improvements are made by increasing the complexity of the twisting motion by the addition of a second control point at mid-span. The resulting twist distribution with two control points shows a relatively large change from root to mid span and a relatively small change from mid-span to the wing-tip. The resulting flapping motion appears to further reduce the presence of instabilities related to separation.

The work here represents an investigation into a small subset of the potentially interesting parameterizations and objective for flapping flight. Fortunately, the optimization framework we use allows for the study of a wide rage of motions and objectives with relatively little modification. Interesting future work for the 2D case includes increasing the complexity of the parameterization by representing the motion via a sinusoidal expansion or piece-wise spline, or to allow for deformation of the airfoil geometry. There are a number of additional parameterization possibilities in 3D as well, include parameterizing the wing planform, allowing more dihedral control points, altering the airfoil section, and allowing for more complex parameter trajectories. The work here also only considers the unconstrained maximization of propulsive efficiency. Finally, an objective perhaps more relative to efficient flight is the minimization of input power given constraints on lift and thrust. This case relates to steady, level flight where the net thrust and lift are zero.

Acknowledgments

This work is supported by the Department of the Army through the Army High Performance Computing Research Center, Cooperative Agreement No. W911NF-07-2-0027, and by the AFOSR under grant no. FA 9550-07-1-0195 from the Computational Math Program under the direction of Dr. Fariba Fahroo. Yves Allaneau is supported by the Hugh H. Skilling Stanford Graduate Fellowship.

References

[1]T. Theodorsen, General Theory of Aerodynamic Instability and the Mechanism of Flutter, *T.R. No. 496*, N.A.C.A., 1935

[2]I. E. Garrick, Propulsion of a Flapping and Oscillating Airfoil, *T.R. No. 567*, N.A.C.A., 1937.

[3]M.J. Lighthill, Hydromechanics of Aquatic Animal Propulsion, *Annu. Rev. of Fluid Mech.*, Vol. 1, p. 413-446, 1969.

[4]T. Weis-Fogh, Quick Estimates of Flight Fitness in Hovering Animals, Including Novel Mechanisms for Lift Production, *J. Exp. Biol.*, Vol. 59, p.169-230, 1973.

[5]P. Liu, A Time-Domain Panel Method for Oscillating Propulsors with Both Chordwise and Spanwise Flexibility, Ph. D. Thesis, University of Newfoundland, 1996.

[6]K. D. Jones and M.F.Platzer, Numerical Computation of Flapping-Wing Propulsion and Power Extraction, *AIAA Paper 97-0826*, 1997.

[7]K. D. Jones, C. M. Dohring and M. F. Platzer, Experimental and Computational Investigation of the Knoller-Betz Effect, *AIAA Journal*, Vol. 36, No. 7, July 1998.

[8]K. D. Jones, T. C. Lund and M. F. Platzer, Experimental and Computational Investigation of Flapping Wing Propulsion for Micro Air Vehicles, *Progress in Aeronautics and Astronautics*, Vol. 195, p. 307-339, 2001.

[9]P. -O. Persson, D. J. Willis and J. Peraire, The Numerical Simulation of Flapping Wings at Low Reynolds Numbers, *AIAA Paper 2010-724*

[10]K. Ou, P. Castonguay and A. Jameson, 3D Wing Simulation with High-Order Spectral Difference Method on Deformable Mesh, *AIAA Paper, Orlando, 2011.*

[11]W. Shyy, Y. Lian, J. Tang, H. Liu, P. Trizila, B. Stanford, L. Bernal, C. Cesnik, P. Friedmann, P. Ifju, Computational Aerodynamics of Low Reynolds Number Plunging, Pitching and Flexible Wings for MAV Applications, *AIAA Paper 2008-523*

[12]R. T. Jones, Wing Flapping with Minimum Energy, *NASA TMJ81174*, 1980.

[13]K. C. Hall and S. R. Hall, Minimum Induced Power requirements for Flapping Flight, *J. Fluid. Mech.*, Vol 323, p. 285-315, 1996.

[14]M. Hamdaoui, J.-B. Mouret, S. Doncieux and P. Sagaut, Optimization of Kinematics for Birds and UAVs using Evolutionary Algorithms, *Proceedings of the World Academy of Science, Engineering and Technology*, Vol. 30, July 2008.

[15]K. Ito, Optimization of Flapping Wing Motion, *ICAS 2002 Congress*, 2002.

[16]K. A. Strang, Efficient Flapping Flight of Pterosaurs, *Ph. D. Thesis*, Stanford University, 2009.

[17]M. Milano and M. Gharib, Uncovering the Physics of Flapping Flat Plates with Artificial Evolution, *J. Fluid Mech.*, Vol. 534, p. 403-409, 2005.

[18]I. H. Tuncer and M. Kaya, Optimization of Flapping Airfoils for Maximum Thrust and Propulsive Efficiency, *Acta Polytechnica*, Vol 44, No. 1, 2004.

[19]D. J. Willis, P. -O. Persson, E. R. Israeli, J. Peraire, S. M. Swartz, K. S. Breuer, Multifidelity Approaches for the Computational Analysis and Design of Effective Flapping Wing Vehicles, *AIAA Paper 2008-518*, 2008.

[20]A. Jameson, The Construction of Discretely Conservative Finite Volume Schemes that Also Globally Conserve Energy or Entropy, *Journal of Scientific Computing*, Vol. 34-2, p. 152-187, 2008

[21]A. Jameson, Formulation of Kinetic Energy Preserving Conservative Schemes for Gas Dynamics and Direct Numerical Simulation of One-Dimensional Viscous Compressible Flow in a Shock Tube Using Entropy and Kinetic Energy Preserving Schemes, *Journal of Scientific Computing*, Vol. 34-2, p. 188-208, 2008

[22]Y. Allaneau and A. Jameson, Direct Numerical Simulations of Plunging Airfoils, *AIAA Paper 2010-728*, January 2010.

[23]Y. Allaneau, M. Culbreth and A. Jameson, A Computational Framework for Low Reynolds Number 3D Flapping Wings Simulations, *AIAA Paper*, Hawaii, 2011.

[24]C. W. Shu, Total Variation Diminishing Time Discretizations, *SIAM Journal on Scientific and Statistical Computing*, Vol. 9, p. 1073-1084

[25]P. E. Gill, W. Murray, and M. A. Saunders, SNOPT: An SQP Algorithm for Large-Scale Constrained Optimization, *SIAM Rev.* Vol. 47-1, 99-131, 2005